A Performance-Based Earthquake Fatality Modeling Framework Using Collapse Volume Ratios

Luis Ceferino[1], Yinchen Yi[1], Wenxiao Li[1], Yvonne Merino[1], Luis Moya[2], Kimberley Shoaf[3], and Emily So[4]

[1]Civil and Environmental Engineering Department, University of California Berkeley, Berkeley, CA, 94720, United States of America
[2]GERDIS Research Group, Department of Engineering, Pontificia Universidad Católica del Perú, Lima, 15088, Peru
[3]Division of Public Health, University of Utah, Salt Lake City, UT 84112, United States of America
[4]Department of Architecture, University of Cambridge, 1-5 Scroope Terrace, Cambridge, CB2 1PX, United Kingdom

October 1, 2025

Email: ceferino@berkeley.edu

Abstract

Conventional earthquake fatality models represent building performance as a binary collapse state, an assumption that overlooks severe failure modes and systematically underestimates fatalities. This study advances the collapse volume ratio—a continuous metric quantifying the reduction of survivable space during collapse—into a probabilistic framework that directly links structural failure to fatality risk. Although previously introduced and quantified in limited studies, we extend its role from an observational measure to an analytical component of performance-based earthquake engineering modeling. The framework is designed for versatility, allowing implementation with different levels of data availability, including site-specific collapse observations, collapse fragility functions, or complete-damage fragility functions. Its applicability is demonstrated by leveraging post-earthquake data from reinforced concrete moment frame buildings affected by the 2023 Kahramanmaraş earthquakes and through case studies of mid-1970s non-ductile and post-1997 ductile concrete space-frame archetypes in California. Results show that conventional approaches, constrained by binary collapse assumptions, may underpredict fatalities by up to fortyfold at high shaking intensities. In contrast, the proposed framework reproduces observed fatality rates, estimating that under Maximum Considered Earthquake shaking, non-ductile buildings may experience fatality

rates of 65%, compared to 11% for ductile buildings. These findings provide quantitative evidence of the life-safety benefits of modern seismic design and highlight the urgent need for retrofit policies addressing older, non-ductile construction.

Collapse volume ratio, earthquake fatalities, non-ductile concrete buildings, performance-based earthquake engineering, seismic retrofits

1 Introduction

Earthquakes cause excessive human consequences, including deaths, injuries, and long-term impacts on affected populations [1, 2, 3, 4, 5, 6]. Fatalities inside buildings are primarily linked to structural damage. Classic studies identified elevated risks for occupants on ground floors, where structural elements carry more loads and are prone to failure [7, 8]. More recent research has shown that casualty outcomes also depend on earthquake characteristics, building use and occupancy patterns, and the speed of rescue and treatment [9, 10].

Structural collapse produces both immediate fatalities through crushing and delayed mortality from untreated injuries [11, 12, 13, 14, 15]. Survivors trapped under debris often face prolonged entrapment, during which severe injuries can worsen without timely rescue or treatment [16, 5]. A key determinant of survival is entrapment time, as extended confinement increases the likelihood of developing crush syndrome and acute renal failure [17]. Hospitalization records show that up to 80% of survivors rescued from collapsed buildings sustain crush syndrome [18], underscoring how structural failures inflict traumatic injuries and shape the medical complications that follow.

Because collapse mechanisms so strongly influence mortality, fatality modeling must account for the structural vulnerabilities that drive these failures. An important portion of the existing building stock remains at high risk of collapse, particularly older reinforced concrete frames built before the mid-1970s in the US and similar pre- and early-code construction worldwide [19, 20, 21, 22, 23, 24]. Non-ductile reinforced concrete buildings lack proper seismic detailing, such as insufficient transverse reinforcement and poor confinement at beam-column joints, which can lead to brittle behavior and rapid collapse [25, 26]. These weaknesses have been repeatedly confirmed in the field, most recently in the 2023 Türkiye–Syria earthquakes, where widespread soft-story and pancake failures were documented [27, 28, 29].

Earthquake casualty models provide the link between such structural vulnerabilities and human consequences [30, 31, 32, 33, 34, 35, 36, 37, 38, 39]. These models typically assume that increasing levels of structural damage correspond to higher rates of injuries and fatalities, with the most severe outcomes associated with building collapse [40, 41]. Consistent with field observations [42, 43, 9, 10], current approaches consider collapse as the dominant mechanism of earthquake fatalities. Accordingly, state-of-the-art frameworks model collapse in a binary fashion—a building either collapses or it does not—and assign fatality rates to collapsed structures based on expert elicitation and sparse post-earthquake data. For instance, widely used methodologies often assume fixed rates such as a 10% fatality ratio for collapsed reinforced concrete moment-frame buildings [41], regardless of the collapse severity (Figure 1) . Modern software tools for casualty estimation, including those used in HAZUS [41] and FEMA P-58 [44, 45] workflows, rely on this binary approach to quantify risks and evaluate the benefits of mitigation strategies such as retrofitting.

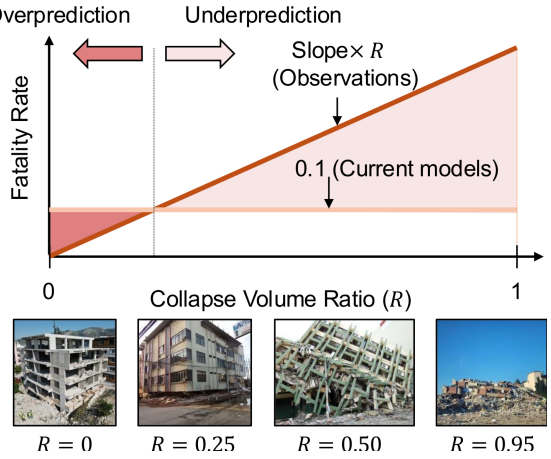

Figure 1: Illustration of the relationship between collapse volume ratio (R) and earthquake fatality rates. The collapse volume ratio ranges from 0 (no collapse) to 1 (complete pancake collapse), representing the fraction of safe space lost within a building. Empirical evidence suggests that fatality risk increases with larger collapse volume ratios, with rates as high as 40–80% observed in near-total collapses for concrete buildings [46], e.g., slope could go from 0.4 to 0.8. The lower horizontal line illustrates the simplifying assumption in current casualty models, where a fixed fatality rate (e.g., 10%) is applied uniformly to all collapsed buildings. Photographs show examples of buildings at different levels of collapse severity and values of R. Photographs were extracted from [5]

While this paradigm represents the current standard in disaster risk modeling, earthquake observations increasingly reveal its limitations [46, 47]. Fatalities are not driven solely by the binary occurrence of collapse, but by the extent of collapse. Safe spaces within buildings are progressively lost as vertical load-bearing elements fail. Localized collapse mechanisms, such as the failure of a single story, place occupants of that story at disproportionately higher risk, while global pancake collapses reduce survivable spaces across all floors. These distinctions are not captured in current binary models, which obscures the structural mechanisms leading to fatalities.

To address this gap, researchers have introduced the concept of the *collapse volume ratio*, a continuous measure of the fraction of safe space lost due to partial or total collapse [7, 48, 49, 9, 47, 50, 10]. This ratio ranges from 0 for a fully standing building to 1 for complete collapse, with intermediate values representing partial collapses (Figure 1). Empirical evidence suggests that higher collapse volume ratios are strongly correlated with increased fatality rates, reaching values of 40–80% in extreme cases [46, 47]. Although data scarcity has prevented precise calibration of this relationship, a linear approximation is reasonable, since the collapse volume ratio is directly proportional to the loss of safe space. Critically, this insight reveals that binary collapse models may substantially underpredict fatalities with their 10% rate, independent of the collapse severity [41].

Despite progress in modeling structural response [51, 44], predicting collapse volume ratios remains challenging. Most fragility models developed over the past decades focus on damage states ranging from slight to complete damage, with limited attention to structural behavior beyond the onset of collapse [52, 53, 20]. Consequently, casualty models lack the

granularity to capture collapse-induced mechanisms of severe injury and death.

At the same time, advances in observational technologies, such as Light Detection And Ranging (LiDAR) and unmanned aerial vehicles (UAVs), provide highly detailed information on collapsed buildings [54, 55, 56, 57, 58]. These capabilities enable systematic exploration of empirical collapse volume ratios and create new opportunities to improve fatality rate estimates.

Although previously introduced and quantified in limited studies [59], we extend the collapse volume ratio from an observational indicator to an analytical component within performance-based earthquake engineering. We propose a modeling framework for earthquake fatalities that explicitly represents the collapse volume ratio and calibrate it using a unique dataset collected after the 2023 Kahramanmaraş Earthquake in Turkey [28]. We begin by diagnosing the limitations of prevailing fatality models, then present three formulations aligned with different levels of data availability: (i) direct collapse observations, (ii) collapse fragility functions, and (iii) complete-damage fragility functions. We then introduce the empirical collapse volume ratio data and the fitted models. Finally, we demonstrate the framework for ductile and non-ductile reinforced concrete frame buildings and discuss implications for risk modeling and retrofit policy.

2 Limitations of Existing Fatality Models

Current earthquake fatality models rely on a binary treatment of structural collapse and are heavily extrapolated from limited data [40, 60, 61, 41]. In this section, we demonstrate the asymptotic properties of such models and highlight how they can substantially underestimate fatalities in collapsed buildings.

Let F be the random variable representing the fatality rate (ratio of deaths to total occupants), where $F \in [0, 1]$. Let DS denote the building's damage state after an earthquake, such that

$$DS \in \{\text{None}, \text{Slight}, \text{Moderate}, \text{Extensive}, \text{Complete}\}.$$

The most severe category, *Complete*, corresponds to irreparable structural damage, which may or may not involve physical collapse. Thus, *Collapse* is a subset of $DS = \text{Complete}$.

Next, let IM denote the intensity measure representing the maximum shaking intensity experienced by the building. Examples include peak ground acceleration (PGA) or spectral acceleration $\text{Sa}(T)$ at the fundamental period T of the structure, such that $IM \in R^+$.

Using the law of total expectation (tower property), the expected fatality rate conditional on shaking intensity can be expressed as:

$$E[F \mid IM] = E\big[E[F|DS] \mid IM\big] = \sum_{DS} E[F \mid DS]\, P(DS \mid IM). \tag{1}$$

Since fatalities occur predominantly in collapsed buildings, the contribution of other damage states is negligible. For example, in HAZUS, the fatality rate for Collapse is set at 0.10 for concrete buildings, whereas the rate for Extensive damage is only 0.0001—a thousand times smaller [41]. Thus, the expectation simplifies to:

$$E[F \mid IM] \approx E[F \mid DS = \text{Complete}] \times P(DS = \text{Complete} \mid IM). \tag{2}$$

In practice, however, most risk models (e.g., HAZUS) do not explicitly model Collapse [41]. Instead, Collapse is treated as a conditional probability within the Complete damage state:

$$E[F \mid IM] \approx E[F \mid \text{Collapse}] \times P(\text{Collapse} \mid DS = \text{Complete}) \times P(DS = \text{Complete} \mid IM). \tag{3}$$

Here, $E[F \mid \text{Collapse}]$ is the fatality rate given collapse, $P(\text{Collapse} \mid DS = \text{Complete})$ is the assumed collapse probability within the Complete state, and $P(DS = \text{Complete} \mid IM)$ is the complete-damage fragility function. Importantly, $P(\text{Collapse} \mid DS = \text{Complete})$ is modeled as a constant, independent of IM [41].

This formulation produces an unrealistic saturation of fatality rates at high shaking levels. When $IM \to \infty$, the probability of complete damage approaches one. Thus,

$$\lim_{IM \to \infty} E[F \mid IM] = E[F \mid \text{Collapse}] \times P(\text{Collapse} \mid DS = \text{Complete}). \tag{4}$$

For reinforced concrete moment-frame medium-rise buildings, HAZUS sets $E[F \mid \text{Collapse}] = 0.1$ and $P(\text{Collapse} \mid DS = \text{Complete}) = 0.1$, yielding an upper fatality rate of only 1% (Figure 2).

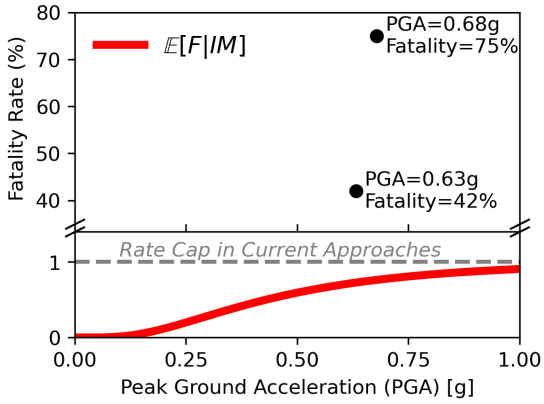

Figure 2: Comparison of the HAZUS fatality model with observed fatality rates from the 2011 Christchurch earthquake. The curve shows the expected fatality rate $E[F \mid IM]$. Black markers represent two reinforced concrete buildings: the CTV building (75% fatality rate at 0.68g) and the PGC building (42% fatality rate at 0.63g) [46].

This saturation at 1% starkly contradicts earthquake observations. In the 2011 Christchurch earthquake, 185 people died, 135 of them in just two reinforced concrete moment-frame buildings. These structures experienced strong shaking (0.63–0.68g) and exhibited high collapse volume ratios, leading to fatality rates of 42% and 75%, respectively [46]. Current fatality models are fundamentally unable to capture such outcomes, as they cap fatality rates at levels forty to seventy times lower (Figure 2).

In the United States, current fatality models are calibrated primarily using data from moderate earthquakes, such as the 1994 Northridge (M_w 6.4) and 1989 Loma Prieta (M_w 6.9) earthquakes [62, 60, 61]. These events caused relatively few building collapses and very few fatalities. Extrapolating fatality rates from such limited events to larger earthquakes

with extensive collapse is problematic. For example, assuming a constant 10% probability of collapse given complete damage ignores the fact that reinforced concrete buildings can experience large collapse volume ratios under strong shaking. As illustrated in Figure 1, this assumption leads to severe underestimation of fatalities in high-intensity events.

In sum, existing fatality models can underestimate earthquake deaths by factors of 40 to 70 (predicting 1% versus observed 42% and 75%) in realistic collapse scenarios, due to their reliance on a binary notion of collapse and calibrations from moderate earthquakes. To overcome this limitation, we first introduce a new model for collapse volume ratios, which then serves as the foundation for developing a more realistic framework for earthquake fatality modeling.

3 A Probabilistic Model for Collapse Volume Ratios

Let R denote the *collapse volume ratio*, interpreted as the fraction of originally safe interior volume rendered unsafe by structural failure. By construction,

$$R \in [0,1], \qquad R = \begin{cases} 0 & \text{no collapse (building stands),} \\ 1 & \text{full/pancake collapse,} \\ r \in (0,1) & \text{partial collapse (e.g., soft-story).} \end{cases} \tag{5}$$

Conditioning on an intensity measure IM, e.g., PGA or Sa(T), we specify R as a mixed discrete–continuous random variable with point mass at 0, point mass at 1, and a continuous density on $(0,1)$ (Figure 3):

$$P(R = 0 \mid IM) = p_0(IM), \tag{6}$$
$$P(R = 1 \mid IM) = p_1(IM), \tag{7}$$
$$f_{R|IM}(r \mid IM) = \big[1 - p_0(IM) - p_1(IM)\big]\, f(r; IM), \qquad r \in (0,1). \tag{8}$$

For brevity, we suppress the explicit dependence on IM in what follows and write p_0, p_1, and $f(r)$ unless ambiguity may arise (Figure 3); all are functions of IM.

The corresponding CDF is

$$F_R(r) = \begin{cases} 0, & r < 0, \\ p_0, & r = 0, \\ p_0 + \big[1 - p_0 - p_1\big]\, F(r), & 0 < r < 1, \\ 1, & r \geq 1, \end{cases} \tag{9}$$

where $F(r) = \int_0^r f(u)\, du$ (Figure 3).

Throughout, we adopt a Beta density for the continuous component:

$$f(r) = \mathrm{Beta}\big(r;\, \zeta, \eta\big) = \frac{r^{\zeta-1}\,[1-r]^{\eta-1}}{B(\zeta,\eta)}, \qquad r \in (0,1), \tag{10}$$

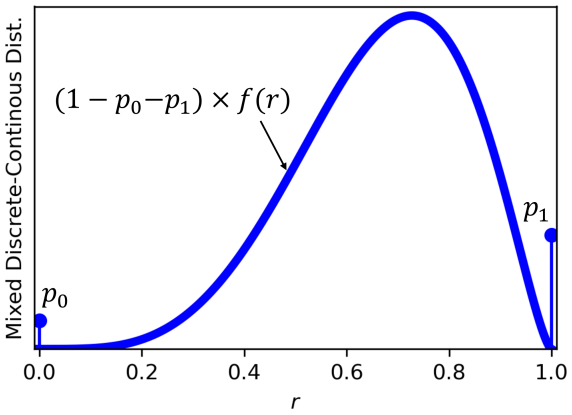

(a) Mixed Mass-Density Probability Distribution

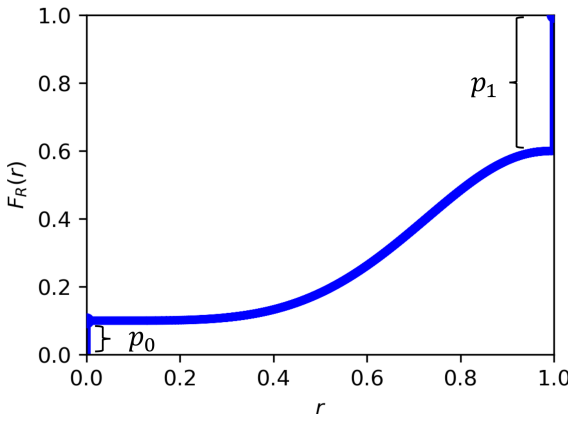

(b) Cumulative Distribuition Fucntion

Figure 3: Mixed discrete–continuous probability model for collapse volume ratios R conditioned on shaking intensity IM. (a) The distribution includes point masses at $R = 0$ (no collapse) and $R = 1$ (full collapse), with a continuous density $(1 - p_0 - p_1)f(r)$ for $0 < r < 1$ (partial collapse). (b) The cumulative distribution shows jumps of size p_0 and p_1 at 0 and 1. Both point probabilities and the density evolve with IM, reflecting how stronger shaking increases collapse likelihood and severity.

where $B(\zeta, \eta)$ denotes the Beta function,

$$B(\zeta, \eta) = \int_0^1 t^{\zeta-1}(1-t)^{\eta-1}\, dt. \tag{11}$$

We employ the mean–precision reparameterization

$$\zeta = \mu\,\phi, \qquad \eta = (1-\mu)\phi, \qquad \mu = \text{logistic}\big(\theta_0 + \theta_1 \ln IM\big), \tag{12}$$

with precision $\phi > 0$, where the logistic function is defined as

$$\text{logistic}(x) = \frac{1}{1+e^{-x}}.$$

This choice flexibly captures shifts in the distribution of the partial-collapse severity with the shaking intensity.

The random event $R > 0$ is equivalent to *Collapse*, representing the sudden and irreversible loss of load-carrying capacity that reduces safe interior space (e.g., through a soft-story failure). Conversely, $R = 0$ corresponds to no collapse. Formally,

$$\{R > 0\} \;\Leftrightarrow\; \{\text{Collapse}\}, \qquad \{R = 0\} \;\Leftrightarrow\; \{\neg\text{Collapse}\}. \tag{13}$$

Since collapse occurs only within the *Complete* damage state, we note that $\{\text{Collapse}\} \subset \{DS = \text{Complete}\}$. For damage states below Complete ($DS \in \{\text{None}, \text{Slight}, \text{Moderate}, \text{Extensive}\}$), the collapse volume ratio is $R = 0$.

To address different levels of data availability and computational workflows, we develop three versions of the collapse volume ratio model: (a) a site-specific model, (b) a model

coupled with collapse fragility functions, and (c) a model coupled with complete-damage fragility functions (Figure 4). The site-specific model is tailored to regions where empirical data on collapse volume ratios are available. The second and third versions are designed for broader applicability: they leverage existing fragility models to generalize the framework beyond single sites, allowing integration with established performance-based earthquake engineering methodologies. This tiered approach acknowledges the scarcity of direct collapse volume ratio data and the current limitations of numerical modeling, while ensuring that the proposed framework can be adapted to both data-rich and data-poor contexts.

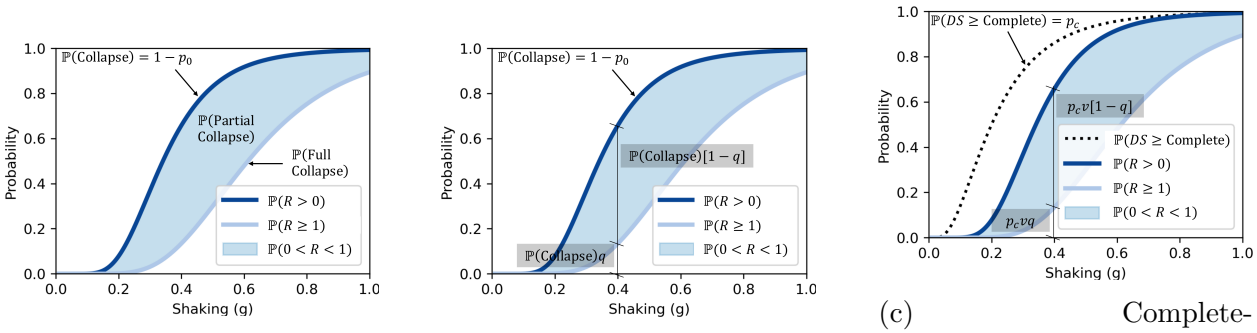

(a) Site-specific model (b) Collapse-coupled model (c) Complete-damage–coupled model

Figure 4: Three formulations of the collapse volume ratio model showing how probabilities of no collapse, partial collapse, and full collapse evolve with shaking intensity. (a) The site-specific model directly estimates these probabilities from regional collapse volume data. (b) The collapse-coupled model links collapse ratios to existing collapse fragility functions (e.g., from advanced structural modeling methodologies) through conditional factors. (c) The complete-damage–coupled model relates collapse ratios to complete-damage fragilities (e.g., HAZUS) also through conditional factors. Together, these models provide flexible pathways to incorporate empirical data, simulations, or legacy fragilities.

3.1 A Site-specific Model

In regions where data on collapse volume ratios are available, we directly calibrate the mixed distribution in (6)–(8). This setting corresponds to a zero–one inflated Beta distribution, where mass probabilities are placed at $R = 0$ (no collapse) and $R = 1$ (full collapse), and a Beta density governs outcomes in $(0, 1)$ (partial collapse).

Here p_0 and p_1 are specified by lognormal fragility functions:

$$p_0 = 1 - \Phi\left(\frac{\ln IM - \ln a_0}{b}\right), \tag{14}$$

$$p_1 = \Phi\left(\frac{\ln IM - \ln a_1}{b}\right), \qquad a_0 < a_1, \tag{15}$$

where $\Phi(\cdot)$ is the standard normal CDF (Figure 4a). The parameters a_0 and a_1 are the median intensity levels at which there is a 50% probability of any collapse ($R > 0$) and of full collapse ($R = 1$), respectively. The parameter b is the logarithmic standard deviation,

assumed equal in both fragility functions to avoid curve cross-overs [63]. The continuous component is given by (10)–(12). Equations (14)–(15) govern the probabilities of no collapse and full collapse as shaking increases, while (12) tunes the distribution of partial collapse severities.

3.2 A Model Coupled with Collapse Fragility Functions

In many regions, direct observations of collapse volume ratios are not available, making it difficult to calibrate site-specific models. A practical alternative is to leverage existing or compute new collapse fragility functions, which are increasingly produced through modern performance-based earthquake engineering (PBEE) methods [20, 51]. Recent PBEE approaches, such as FEMA P-58 [44, 45], combine advanced computational models with extensive experimental data on structural components. These methods enable explicit simulation of collapse onset, identifying when dynamic instabilities occur (e.g., soft-story or sidesway mechanisms) or when vertical load-carrying elements experience drifts and deformations that exceed their capacity. As a result, collapse fragility functions have become more widely available than collapse volume ratio data and provide a valuable entry point for extending our framework.

To adapt to this setting, we formulate the collapse volume ratio as a *conditional probability model given collapse*. Specifically, rather than using a zero–one inflated Beta distribution (as in the site-specific case), we use a conditional one-inflated Beta distribution (Figure 4b). This reflects the fact that once collapse occurs ($R > 0$), the distribution of outcomes can be split between partial and full collapse.

We define the collapse fragility function as

$$P(\text{Collapse} \mid IM) = P(R > 0 \mid IM) = 1 - p_0. \tag{16}$$

Notice that the parameters of this fragility function are given by the median a_0 and lognormal standard deviation b defined in Equation 14. We also define the conditional transition to full collapse as

$$q(IM) = P(R = 1 \mid R > 0, IM) = \Phi\left(\frac{\ln IM - \ln \alpha}{\beta}\right), \tag{17}$$

where α is the median shaking intensity at which the probability of full collapse becomes 50%, and β is the logarithmic standard deviation. Here both terms depend on IM, but we suppress it for brevity.

The resulting mixture weights are

$$\begin{aligned} P(R = 0 \mid IM) &= p_0 = 1 - P(\text{Collapse} \mid IM), \\ P(R = 1 \mid IM) &= p_1 = P(\text{Collapse} \mid IM)\, q, \\ P(0 < R < 1 \mid IM) &= P(\text{Collapse} \mid IM)\,[1 - q], \end{aligned} \tag{18}$$

and the partial-collapse distribution remains a Beta regression as in (10)–(12).

This formulation has two important features (Figure 4b). First, it generalizes the site-specific model by coupling with collapse fragility curves, which can be derived from numerical

simulations or empirical studies in other regions. Second, the factor q acts as a multiplicative adjustment: it modulates the distribution of collapse volume ratios so that it reflects regional differences in collapse probabilities and vulnerabilities. As a result, the functional form of p_1 differs from the site-specific case (here it is expressed as the product of two fragility functions), but this trade-off yields broader applicability in data-scarce settings.

3.3 A Model Coupled with Complete Damage Fragility Functions

A third version of the model leverages the large libraries of *complete-damage fragility functions* that were developed in earlier generations of performance-based earthquake engineering. Historically, approaches such as the capacity-spectrum method used pushover curves and spectral displacement estimates to define damage states [64]. These simplified, static procedures allowed for computationally efficient modeling, enabling the creation of extensive catalogs of fragility functions in tools such as HAZUS [41]. As a result, complete-damage fragilities are widely available across regions and structural types, and continue to underpin many regional risk assessments.

The main limitation of these older models is that they cannot explicitly reproduce local collapse mechanisms (e.g., soft-story failures), which are critical for casualty estimation. Instead, they treat *Complete* damage as a broad state encompassing both irreparable but standing structures and those that have collapsed. Consequently, simplified conversions have been used to approximate collapse rates within the complete-damage state, but these ignore shaking intensity and cannot capture variation in collapse severity. Our formulation addresses this gap by introducing collapse volume ratios within the complete-damage framework.

We define the probability of reaching the complete-damage state as

$$P(DS \geq \text{Complete} \mid IM) = p_c(IM) = \Phi\left(\frac{\ln IM - \ln a_c}{b_c}\right), \tag{19}$$

where a_c and b_c are the median and logarithmic standard deviation of the fragility. Conditional on $DS \geq$ Complete, we introduce two transitions:

$$\begin{aligned} v(IM) &= P(R > 0 \mid DS \geq \text{Complete}, IM) = \Phi\left(\frac{\ln IM - \ln \lambda}{\gamma}\right), \\ q(IM) &= P(R = 1 \mid R > 0, IM) = \Phi\left(\frac{\ln IM - \ln \alpha}{\beta}\right), \end{aligned} \tag{20}$$

where λ, γ govern the transition from standing-but-complete-damage to collapse, and α, β govern the transition from collapse onset to full collapse. Here, p_c, v, and q depend on IM, but we suppress it for brevity as well. Also, notice that q is the same as the one in the model coupled with Collapse fragility functions (Figure 4c).

The resulting mixture weights are

$$\begin{aligned} P(R = 0 \mid IM) &= 1 - p_c\, v, \\ P(R = 1 \mid IM) &= p_c\, v\, q, \\ P(0 < R < 1 \mid IM) &= p_c\, v\, [1 - q], \end{aligned} \tag{21}$$

and the continuous partial-collapse distribution is again modeled using the Beta regression of (10)–(12).

This formulation extends the applicability of our model to settings where only complete-damage fragility functions are available, as in HAZUS (Figure 4c). It preserves compatibility with legacy fragility libraries, while embedding collapse volume ratios as a richer measure of failure severity. A key difference relative to the site-specific model is that the functional forms of p_0 and p_1 now involve products of lognormal fragility functions rather than single ones. The benefit, however, is wide generalization: calibrated parameters from one structural class (e.g., non-ductile concrete frames) can be combined with complete-damage fragilities for other classes, allowing the distribution of collapse volume ratios to flexibly capture regional variations in collapse tendencies even in data-poor contexts.

3.4 Parameter Estimation

The three formulations introduced above can all be estimated from data using maximum likelihood. Let $\mathcal{S} = \{(R_i, IM_i)\}_{i=1}^{m}$ denote a sample of collapse volume ratios with associated shaking intensities. Estimation naturally separates into two components: first, the parameters governing the probabilities of no collapse and full collapse are fitted using all data; second, the Beta regression parameters are obtained using only the subset of observations in the partial-collapse range.

Discrete probabilities. For all three model versions, the fragility-based probabilities of $R = 0$ and $R = 1$ are fitted with the full dataset.

Site-specific model. Here p_0 and p_1 are given by (14)–(15), parameterized by (a_0, a_1, b). The log-likelihood is

$$\ell(a_0, a_1, b) = \sum_{i=1}^{m} \Big[I\{R_i = 0\} \ln p_0(IM_i) + I\{R_i = 1\} \ln p_1(IM_i) + I\{R_i \in (0,1)\} \ln \big(1 - p_0(IM_i) - p_1(IM_i)\big) \Big].$$

Collapse-coupled model. In this case, the event $R > 0$ corresponds to collapse. The collapse fragility $P(\text{Collapse} \mid IM)$ is first estimated using

$$\ell(a_0, b) = \sum_{i=1}^{m} \Big[I\{R_i = 0\} \ln p_0(IM_i) + I\{R_i > 0\} \ln(1 - p_0(IM_i)) \Big].$$

Conditional on $R > 0$, the transition to full collapse is modeled by $q(IM)$ with parameters (α, β), estimated using the subset $\bar{\mathcal{S}} = \{R_i > 0\}$:

$$\ell(\alpha, \beta) = \sum_{i \in \bar{\mathcal{S}}} \Big[I\{R_i = 1\} \ln q(IM_i) + I\{R_i \in (0,1)\} \ln(1 - q(IM_i)) \Big].$$

Complete-damage–coupled model. Here the probability of reaching the complete-damage state is first fitted using observed damage states or catalog fragilities:

$$\ell(a_c, b_c) = \sum_{i=1}^{m} \Big[I\{DS_i \geq \text{Complete}\} \ln p_c(IM_i) + I\{DS_i < \text{Complete}\} \ln(1 - p_c(IM_i)) \Big],$$

with $p_c(IM) = P(DS = \text{Complete} \mid IM)$ defined by parameters a_c and b_c in Equation 19. Conditional on $DS \geq$ Complete, the probability of collapse is governed by $v(IM) = P(R > 0 \mid DS \geq \text{Complete}, IM)$, with parameters (λ, γ) estimated through

$$\ell(\lambda, \gamma) = \sum_{i:DS_i \geq \text{Complete}} \Big[I\{R_i = 0\} \ln(1 - v(IM_i)) + I\{R_i > 0\} \ln v(IM_i) \Big].$$

The transition from partial to full collapse, $q(IM)$, is then estimated in the same way as in the collapse-coupled model.

Beta regression. The Beta regression parameters $(\theta_0, \theta_1, \phi)$ are fitted using only the partial-collapse cases $\{R_i \in (0, 1)\}$. With $\mu(IM) = \text{logistic}(\theta_0 + \theta_1 \ln IM)$, the log-likelihood is

$$\ell(\theta_0, \theta_1, \phi) = \sum_{R_i \in (0,1)} \Big[(\mu_i \phi - 1) \ln R_i + ((1 - \mu_i)\phi - 1) \ln(1 - R_i) - \ln B\big(\mu_i \phi, (1 - \mu_i)\phi\big) \Big],$$

where $\mu_i = \mu(IM_i)$ from Equation 12 and $B()$ the Beta function from Equation 11.

This separation ensures that the full dataset informs the probabilities of no collapse and full collapse, while the Beta regression is calibrated only on observations that characterize the distribution of partial collapses.

4 Empirical Data on Collapse Volume Ratios

We assembled a unique dataset on collapse volume ratios for reinforced concrete buildings affected by the 2023 Kahramanmaraş earthquakes in Türkiye [28]. The dataset is based on detailed visual inspections of virtual records of damaged buildings in Antakya, Gaziantep, and Malatya—cities with large stocks of medium-rise reinforced concrete moment-resisting frame apartment buildings. These typologies were confirmed by the authors during multiple post-earthquake deployments. Both the 4:17 am (UTC+3) M 7.8 and the 1:24 pm (UTC+3) M 7.7 earthquakes produced high levels of shaking in these regions [65, 66]. Figure 5 and Supplementary Figure 1 show the distribution of peak ground accelerations (PGA) and spectral accelerations at period of vibration of 1.0 second (Sa[1.0]) for these two events, respectively.

These cities contain thousands of medium-rise multi-family buildings, predominantly reinforced concrete moment frames. To document collapse volume ratios in this building stock, we combined two complementary sources of information, allowing us to capture both localized collapse mechanisms and broader regional patterns (Figure 6).

(1) Online video footage. We compiled publicly available videos of damaged buildings that had sufficient resolution to determine collapse mechanisms. In particular, we used footage where the number of collapsed stories could be clearly identified (e.g., Fig. 6). Eight online sources, including two drone-based YouTube videos, provided information on 323 buildings from Antakya and Malatya [67, 68, 69, 70, 71, 72, 73, 74]. Most footage was acquired within three days of the earthquakes, preserving the immediate post-event conditions before debris removal.

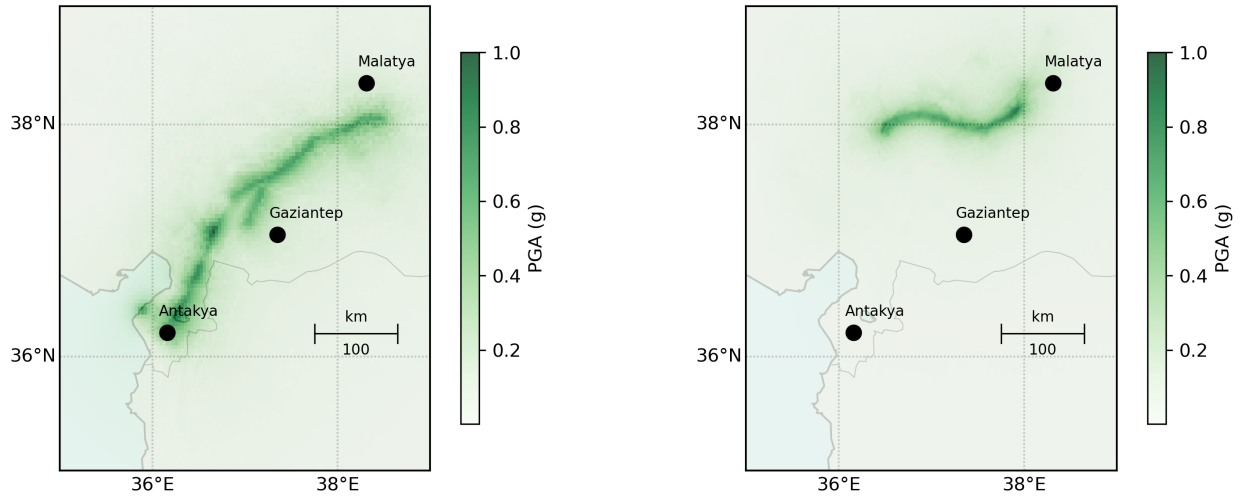

(a) M 7.8 Earthquake

(b) M 7.7 Earthquake

Figure 5: Peak ground accelerations (PGAs) from the 2023 Kahramanmaraş earthquakes. Panels show shaking for (a) the M 7.8 and (b) the M 7.7 events, respectively. The shaking estimates were obtained through USGS ShakeMaps. Collapse volume ratios were extracted for buildings located in Antakya, Gaziantep, and Malatya, highlighted on the maps.

(2) Satellite Imagery. To complement the video dataset, we used high-resolution satellite images covering a neighborhood with 33 concrete buildings in Gaziantep [75], which experienced comparatively lower shaking. By comparing pre- and post-event imagery, we could reliably distinguish between fully standing buildings ($R = 0$) and complete pancake collapses ($R = 1$). However, partial collapses ($0 < R < 1$) could not be consistently identified from satellite data.

Combining both sources yielded 467 buildings with usable collapse information. To refine classifications, we performed an additional step for buildings that remained fully standing immediately after the earthquake (Figure 7). Using updated satellite imagery from May 2025, we distinguished between (i) buildings repaired and still standing ($DS < \text{Complete}, R = 0$) and (ii) buildings later demolished due to structural or financial infeasibility ($DS \geq \text{Complete}, R = 0$).

We further obtained the original number of stories for each building using Google Street View records. The initial dataset contained 467 buildings, but we excluded one- and two-story structures and buildings taller than seven stories to focus on medium-rise reinforced concrete buildings as defined in HAZUS [41]. The final dataset consists of 356 buildings, with an average height of 4.7 stories and a standard deviation of 1.1. (Figure 7).

For each building, the collapse volume ratio was computed as

$$R = \frac{x}{n},$$

where n is the total number of stories and x is the number of collapsed stories. Events were classified into mutually exclusive categories: $DS < \text{Complete}$, $R = 0$, $0 < R < 1$, and $R = 1$ (Figure 7).

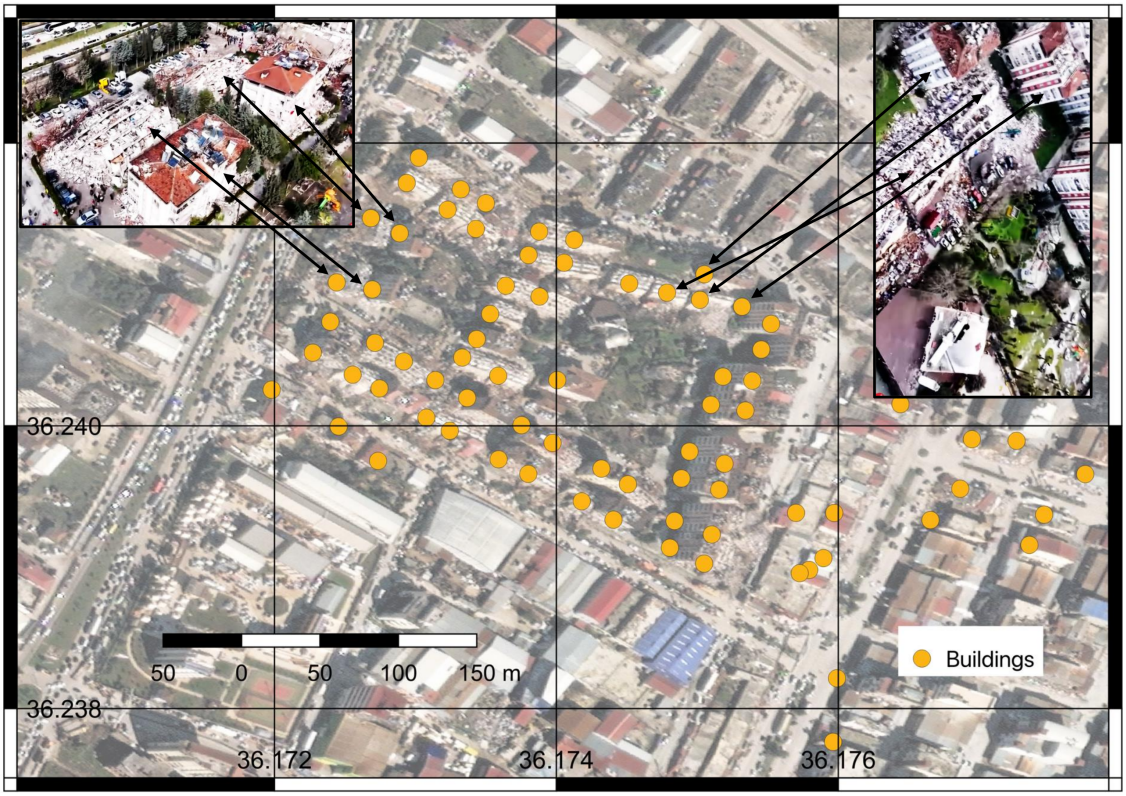

Figure 6: Example integration of satellite imagery (background map) and online video footage (insets) to document collapse mechanisms. Orange dots mark individual buildings identified in the satellite image, while the inset frames show drone footage that enabled estimation of the number of collapsed stories and computation of collapse volume ratios.

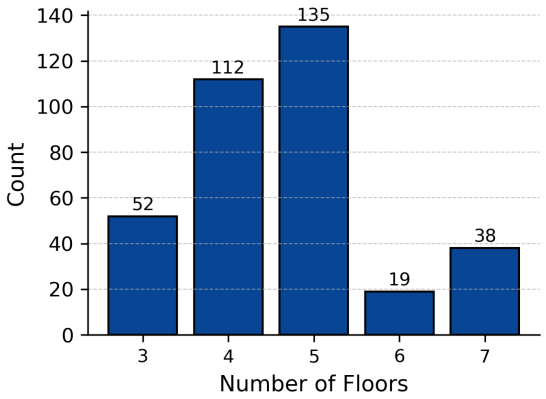

(a) Number of floors in buildings

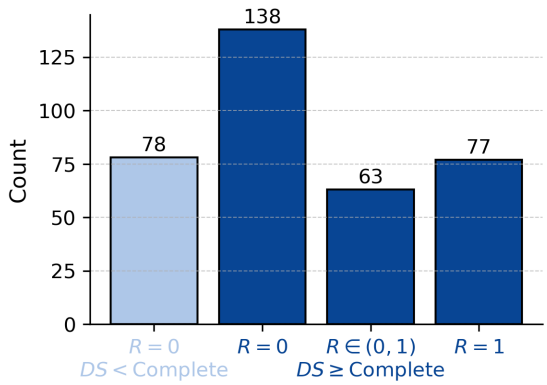

(b) Collapse volume ratio R

Figure 7: Distribution of number of floors and collapse volume ratios (R) in the dataset. Collapse ratios were categorized into $R = 0$ (no visible collapse), $0 < R < 1$ (partial collapse), and $R = 1$ (complete collapse). These classifications form the basis for fragility modeling.

Finally, ground shaking was estimated at each building site using ShakeMap data obtained directly from the USGS API [76]. We extracted peak ground acceleration (PGA) and spectral accelerations at building locations. We also extracted spectral accelerations at 1 second. Details of the interpolation methods are documented in the USGS ShakeMap technical references [77]. Figure 8 and Supplementary Figure 2 show the scatter plots of R versus PGA and versus Sa[1.0], respectively.

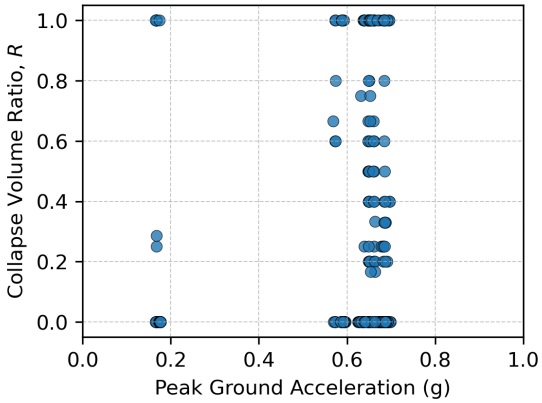

Figure 8: Relationship between peak ground acceleration (PGA) and collapse volume ratio (R) across all regions. Blue markers represent individual buildings with valid damage observations, where $R = 0$ indicates that the building is fully standing, $0 < R < 1$ indicates partial collapse, and $R = 1$ indicates complete collapse.

5 Fitted Collapse Volume Ratio Model

We estimated all model parameters using maximum likelihood estimation (MLE), as described previously. Because the data were not uniformly distributed across shaking levels, we incorporated weights into the log-likelihood function to ensure a good fit across the full intensity range. To compute these weights, we divided the shaking intensity into four equal-width intervals. For PGA, the range was 0.1–0.9 g, and for Sa[1.0], the range was 0–2.0 g. Each data point within an interval was assigned a weight inversely proportional to the number of observations in that interval. This approach balanced the contribution of data-sparse and data-dense regions.

For the parameters α and β that define q (Equation 17), the likelihood function was ill-conditioned due to the scarcity of partial-collapse observations in the dataset. With a larger dataset, these parameters could be robustly estimated using the same MLE framework established earlier. In the present study, however, we addressed this limitation by calibrating the collapse-coupled model to align with the shaking intensities at which the site-specific model yields $P(R \geq 1) = 0.25$ and $P(R \geq 1) = 0.25$. Solving the resulting two-equation system provided consistent values for *alpha* and β, while all other model parameters were obtained directly through MLE.

The resulting parameter estimates are reported in Table 1 for the three model formulations as a function of PGA. Figure 9 shows that $P(R > 0)$ and $P(R \geq 1)$ both increase

monotonically with shaking intensity, and—as expected—do not cross, since $R = 1 \subset R > 0$. The three fitted versions yield comparable results. For example, at 0.5 g, $P(R > 0)$ equals 0.36, 0.38, and 0.46, while $P(R \geq 1)$ equals 0.23, 0.22, and 0.27. These small differences reflect the distinct formulations underlying each model. Table 2 and Supplementary Figure 3 present analogous results for Sa[1.0].

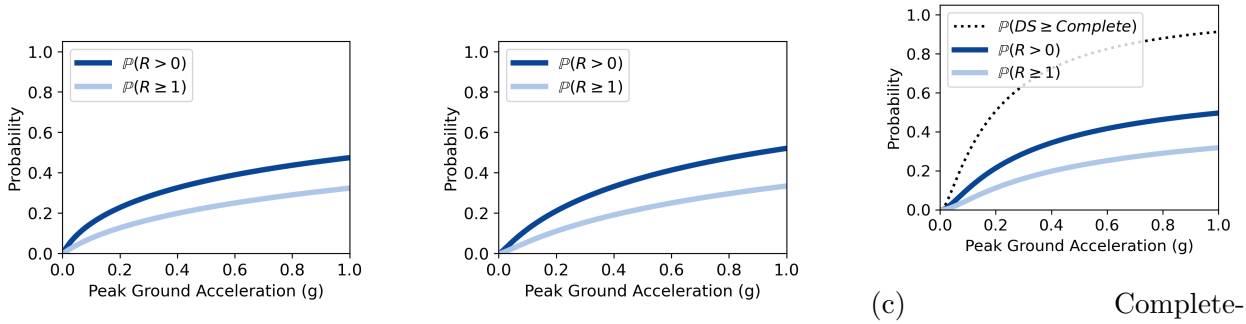

(a) Site-specific model (b) Collapse-coupled model (c) Complete-damage–coupled model

Figure 9: Fitted collapse-volume-ratio (R) models. Maximum-likelihood fits show the probability that $R > 0$ (any collapse; dark blue) and $R = 1$ (full collapse; light blue) versus peak ground acceleration (PGA).

Table 1: Fitted parameters of collapse-volume-ratio (R) models with respect to peak ground acceleration (PGA). Maximum-likelihood estimates are reported for the three formulations—(a) site-specific, (b) collapse-coupled, and (c) complete-damage–coupled.
$^{(*)}$ These numbers were computed by equaling probability targets to the site-specific model instead of MLE.

Parameters	a_c [g]	b_c	a_0 [g]	a_1 [g]	b	α [g]	β	γ	λ	θ_0	θ_1	ϕ
Site specific	–	–	1.16	2.95	2.36	–	–	–	–	-0.13	0.43	11.55
Collapse	–	–	0.91	–	1.88	$0.15^{(*)}$	$5.31^{(*)}$	–	–	-0.13	0.43	11.55
Complete	0.20	1.20	–	–	–	$0.15^{(*)}$	$5.31^{(*)}$	0.56	5.26	-0.13	0.43	11.55

Furthermore, we examine how the average value μ of the Beta distribution $f(r)$ evolves with shaking intensity. Figure 10 and Supplementary Figure 4 show the fitted relationships as a function of PGA and Sa[1.0], respectively, for cases where $R \in (0, 1)$. These results allow us to track not only changes in the mean μ but also in the variance, given by $\mu(1-\mu)/(1+\phi)$. Tables 1 and 2 report the corresponding fitted parameters for the Beta regression as well. The positive values of θ_1 confirm that μ increases with shaking intensity. By construction, the formulation ensures the expected limits: $\lim_{IM\to 0} \mu = 0$ and $\lim_{IM\to\infty} \mu = 1$.

Table 2: Fitted parameters of collapse-volume-ratio (R) models with respect to spectral acceleration at 1.0 seconds (Sa[1.0]). Maximum-likelihood estimates are reported for the three formulations—(a) site-specific, (b) collapse-coupled, and (c) complete-damage–coupled. $^{(*)}$ These numbers were computed by equaling probability targets to the site-specific model instead of MLE.

Parameters	a_c [g]	b_c	a_0 [g]	a_1 [g]	b	α [g]	β	γ	λ	θ_0	θ_1	ϕ
Site specific	–	–	2.77	7.33	2.41	–	–	–	–	-0.30	0.35	7.11
For Collapse	–	–	2.37	–	2.10	$0.33^{(*)}$	$4.99^{(*)}$	–	–	-0.30	0.35	7.11
For Complete	0.37	1.39	–	–	–	$0.33^{(*)}$	$4.99^{(*)}$	1.90	6.35	-0.30	0.35	7.11

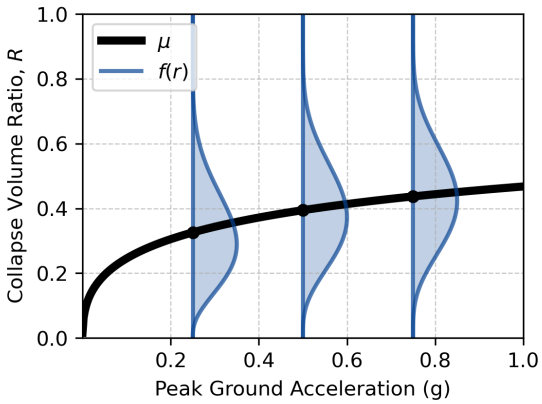

Figure 10: Beta regression fit for collapse volume ratio (R) as a function of peak ground acceleration (PGA). The black curve shows the fitted mean μ, while the blue densities $f(r)$ illustrate the conditional distribution of R at selected PGA levels. The model captures both the expected trend and variability in collapse severity with increasing shaking.

Next, we computed the expected value of R given the intensity measure IM. From the definition of our model

$$E[R|IM] = 0 \times P(R = 0 \mid IM) + \int_0^1 r \times f(r) P(R \in (0,1)|IM) dr + 1 \times P(R = 1|IM)$$

We can eliminate the first term. In the second term, $P(R \in (0,1) \mid IM)$ can be taken outside the integral, leaving only r and $f(r)$ inside. The integral then simplifies to the mean of the Beta distribution, μ. The third term equals p_1. Altogether:

$$E[R|IM] = \mu \times (1 - p_1 - p_0) + p_1 \tag{22}$$

As discussed in the modeling section, p_0 and p_1 are defined differently across model versions, but once obtained, the same expression provides the expected collapse volume ratio.

Using this formulation, we computed $E[R \mid IM]$ for all three models. The expected value increases monotonically with IM for both PGA- and Sa[1.0]-based predictions (Figure 11 and Supplementary Figure 5). Across the full range of ground motions, the three model versions produce nearly identical results. This suggests that, in practice, the choice among model formulations may have little impact on outcomes. Instead, modelers can select the formulation that best aligns with the information available—for example, site-specific curves if sufficient data exist, models coupled with collapse fragilities when structural simulations provide those estimates, or models based on complete damage fragilities if those functions are available.

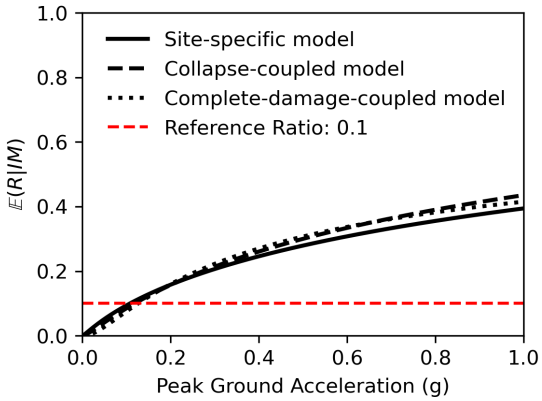

Figure 11: Expected collapse volume ratio $E[R \mid IM]$ as a function of peak ground acceleration (PGA). The curves show predictions from the three formulations: site-specific (solid), collapse-coupled (dashed), and complete-damage–coupled (dotted). The red dashed line marks a reference ratio of $R = 0.1$. All models indicate increasing collapse severity with shaking, with close agreement across formulations.

We also compared our estimates of $E[R \mid IM]$ with current practice. HAZUS, based largely on expert judgment in the U.S., reports collapse probabilities that effectively correspond to average collapse ratios between 0–15% (Table 12-8 in [41]). For reinforced concrete moment-resisting frames, HAZUS prescribes a fixed 10% ratio across all shaking levels. Our results show that this assumption severely underestimates collapse severity. Expected ratios fall below 10% only at very small PGAs (e.g., below 0.1 g). At higher shaking levels, they rise sharply. At 1.0 g PGA, the three models predict expected ratios between 0.39 and 0.44—almost four times greater than the HAZUS value. This is consistent with observations from past earthquakes; for example, in the 2011 Christchurch earthquake, the PGC and CTV buildings exhibited R values of 0.6 and 0.8, respectively [46].

6 A New Probabilistic Model for Fatality Estimation

We develop a new probabilistic model for estimating fatality risk, building on the collapse volume ratio (R) framework. To compute $E(F \mid IM)$ through R, we require a relationship between fatalities (F) and collapse volume ratio. Prior work by So et al. [47, 10, 46]

compiled the limited global datasets relating F and R. Although no theoretical form has been established, we adopt a simple linear relationship:

$$E[F|R] = \kappa R \tag{23}$$

This assumption interprets R as a proxy for the loss of survivable space during partial or total structural collapse, implying fatalities rise in direct proportion to R. In the absence of collapse ($R = 0$), the model predicts zero fatalities. While some trauma injuries leading to fatalities can occur in non-collapsed buildings, these are more appropriately addressed by models of nonstructural damage or background shaking-related injury rates. Here, we restrict attention to fatalities caused by building-collapse-induced trauma.

With this functional form, fatalities can be expressed as a function of ground shaking through the tower property:

$$E[F|IM] = E\big[E[F|R]|IM\big] = E[\kappa R|IM] \tag{24}$$

Using results from Eq. 22 and the linear properties of expectation, we can compute

$$E[F|IM] = \kappa(\mu \times (1 - p_1 - p_0) + p_1) \tag{25}$$

This formulation captures fatalities arising specifically from collapse.

To calibrate the proportionality constant κ, we regressed observed fatality rates against collapse volume ratios for reinforced concrete mid-rise buildings with documented outcomes: the PGC (5-story) and CTV (6-story) buildings from the 2011 Christchurch earthquake (New Zealand) and a 6-story building from the 1999 Foggia earthquake (Italy) [**? ?**]. The observed pairs are $(R, F) = (0.6, 0.42), (0.8, 0.75), (0.9, 0.88)$. Using least squares with the slope constrained through the origin, we obtained $\kappa = 0.91$. This value provides the best fit between collapse volume ratio and fatality rate for concrete buildings; other typologies (e.g., timber) are expected to yield lower slopes.

6.1 HAZUS significantly underestimates fatality rates

We first estimated fatality rates for pre-code (non-ductile) reinforced concrete moment-frame medium-rise buildings using HAZUS [41]. Pre-code buildings refer to pre-1941 structures constructed before modern seismic design requirements were introduced, when ductility and detailing provisions were largely absent. As a result, these buildings are especially vulnerable to brittle failure once their strength limits are exceeded. Medium-rise concrete buildings in HAZUS correspond to 4–7 stories. We applied the lognormal fragility functions for complete damage (Table 5.40 in HAZUS [41]), based on peak ground acceleration (PGA). To compute fatalities, HAZUS assumes a uniform collapse volume ratio of 10% across all shaking intensities and a 10% fatality rate given collapse. As illustrated in Figure 2, this results in fatality rates that increase asymptotically but remain below 1%.

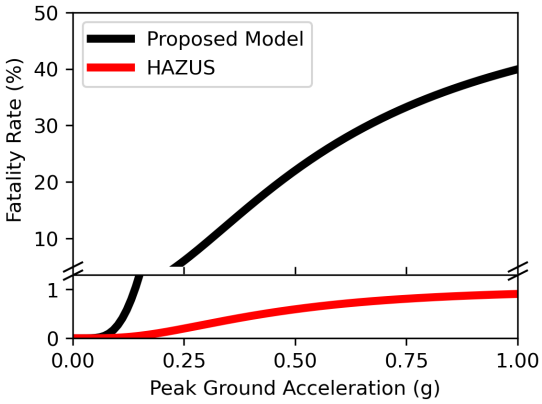

Figure 12: Comparison of predicted fatality rates from the proposed collapse volume ratio–based model (black) and HAZUS estimates (red) as a function of peak ground acceleration (PGA). The proposed model shows a sharp increase in fatality rates with shaking intensity, reaching values above 40% at 1.0 g, while HAZUS assumes substantially lower rates that do not exceed 1%.

We then applied our complete-damage–coupled model using the same HAZUS fragility functions for complete damage in mid-rise non-ductile concrete frame buildings. From Equation 20, we computed v and q, then used these together with the complete damage fragility to estimate p_0 and p_1 from Equation 21. We determined μ from Equation 12, and finally computed $E[F|IM]$ from Equation 25.

Our model produces markedly higher fatality rate estimates than HAZUS. At 1.0 g PGA, the proposed approach predicts a fatality rate of 39.9%, compared with 0.9% from HAZUS—a 44-fold difference (Figure 12). Moreover, comparison with observed cases highlights that actual fatality rates can exceed even our estimates. For example, during the 2011 Christchurch earthquake, the CTV building reached a 75% fatality rate at only 0.68 g, and the PGC building reached 42% at 0.63 g [46]. These comparisons underscore that existing approaches, such as HAZUS, substantially underestimate fatality rates in vulnerable buildings, especially under strong shaking.

6.2 Fatality risks in non-ductile versus ductile concrete buildings

Finally, we study fatality risk in non-ductile versus ductile buildings using modern fragility functions derived from advanced structural modeling for California. A prior study by Liel et al. developed fragility functions for a range of reinforced concrete moment-frame archetypes designed in Los Angeles, California [22, 23]. In our analysis, we focused on their four-story space-frame case: a non-ductile frame designed to the 1967 Uniform Building Code (typical of pre-1970s construction) and a ductile frame designed to ASCE 7-02 and ACI 318-05 provisions for high-seismic regions [23]. Their estimated first-mode periods are 0.94 s for the ductile archetype and 2.0 s for the non-ductile archetype.

For each archetype, Liel et al. developed collapse fragility functions using nonlinear frame models built in OpenSEES [23]. These models captured material nonlinearities, joint behavior, and large deformation effects, and were calibrated to experimental data. Collapse

capacity was then assessed through incremental dynamic analysis (IDA), subjecting the frames to suites of ground motions scaled to increasing intensities.

We adopt the collapse-coupled version of our collapse volume ratio model to study these archetypes. Because the ductile and non-ductile frames have different vibration periods, we expressed the results at a common reference period by converting them to the Sa[1.0]. This was done using the collapse margins reported in [23], defined as the ratio between the median collapse capacity and the spectral acceleration corresponding to the Maximum Credible Earthquake (MCE), i.e., with a probability of exceedance of 2% in 50 years. Specifically, we multiplied the Sa[1.0] at the MCE level (0.79g) by the reported collapse margin (Table 3 in [23]) to obtain the median collapse capacity at that period: 0.53 for mid-1970s (non-ductile) buildings and 2.56 for post-1997 (ductile) buildings. The resulting lognormal fragility functions were defined with these medians and logarithmic standard deviations of 0.64 for the non-ductile case and 0.63 for the ductile case.

Using Equations 21 and 25, we determined $E[F|IM]$. We identified stark differences in fatality risk between ductile and non-ductile buildings. At Sa[1.0]=1.09g —corresponding to current MCE demands in the updated ASCE 7-22 provisions [78]—the estimated fatality rates diverge sharply: 11% for ductile buildings versus 65% for non-ductile buildings. This hazard level is higher than the 0.79g MCE value from the ASCE 7-02 provisions used in the original fragility studies [23], yet the trends remain consistent: post-1997 ductile buildings exhibit relatively controlled collapse probabilities of 16% (only slightly above the 10% design target), whereas non-ductile buildings exceed 93% collapse probability (Supplementary Figure 6) [23]. These findings are also consistent with past earthquake observations, where widespread failures of non-ductile concrete frames produced catastrophic losses while more modern, ductile designs fared significantly better [20]. Taken together, the results underscore the urgent importance of retrofitting non-ductile buildings, as their presence drives an almost tenfold increase in fatality risk—from 11% to 65%—and represents a persistent life-safety gap in the built environment.

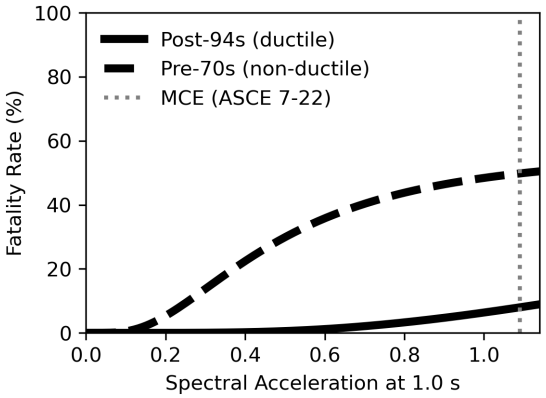

Figure 13: Estimated fatality rates for ductile (post-1994) and non-ductile (pre-1970s) reinforced concrete space-frame archetypes as a function of spectral acceleration at 1.0 s. Results show that, at the MCE level defined in ASCE 7-22 (Sa[1.0] = 1.09g, dashed line), fatality risk is an order of magnitude higher in non-ductile frames (64%) compared to ductile frames (10%). These findings highlight the life-safety benefits of modern seismic design and the urgent need for retrofitting vulnerable non-ductile buildings.

Conclusions

We developed a new modeling framework to predict earthquake fatalities arising from the collapse of buildings. Unlike existing methodologies, this framework explicitly incorporates *collapsed volumes*, a key variable empirically linked to fatality rates in past earthquakes.

The framework was implemented in three versions to accommodate different levels of data availability: (1) site-specific data, (2) collapse fragility functions, and (3) complete-damage fragility functions. This versatility allows direct coupling with established performance-based earthquake engineering workflows, including HAZUS and FEMA P-58.

Our results highlight a major limitation of current fatality models: they asymptotically saturate at unrealistically low rates (e.g., $\sim$1% in HAZUS at high shaking intensities), contradicting field observations of much higher fatality rates in reinforced concrete buildings, for example, 42% and 75% for two collapsed buildings during the Christchurch Earthquake. By explicitly modeling collapsed volumes, our framework avoids this saturation and more closely reproduces observed outcomes. In particular, we showed that current approaches can underpredict fatality rates by up to a factor of 44 for non-ductile concrete buildings.

We further demonstrate the versatility of our framework by applying a version that integrates state-of-the-art structural modeling techniques for California buildings. Using this approach, we estimate that under Maximum Considered Earthquake (MCE) shaking, mid-1970s non-ductile concrete buildings exhibit fatality rates of about 65%, whereas post-1997 ductile buildings show much lower rates, on the order of 11%. These results underscore the life-safety benefits of modern seismic design in California and highlight that retrofit policies targeting older, non-ductile construction can prevent far more fatalities than previously recognized, as earlier models may underestimate fatality risk by up to fortyfold.

Acknowledgements

The authors thank Dr. David Wald of the USGS for his support in computing ShakeMap values at the building sites. This research was supported by the National Science Foundation (Grant No. CMMI-2410291 and CMMI-2410292). The authors also acknowledge the use of large language models (LLMs) to assist with grammar correction and readability improvements.

Conflict of interest

The authors declare no conflict of interest.

Supporting Information

Supplementary Figures 1 to 6 are included in the Supplementary information file. The data and code to reproduce this study can be found in `https://doi.org/10.17603/ds2-kv4c-db15`.

References

[1] Kimberley I. Shoaf et al. "Injuries as a result of California earthquakes in the past decade". In: *Disasters* 22.3 (1998). ISBN: 0361-3666 (Print)\r0361-3666 (Linking), pp. 218–235. ISSN: 03613666. DOI: 10.1111/1467-7717.00088. URL: http://www.ncbi.nlm.nih.gov/pubmed/9753812.

[2] Kimberley Shoaf and Steven Rotiman. "Public Health Impact of Disasters". en. In: *The Australian Journal of Emergency Management* 28.3 (2000).

[3] C Peek-Asa. "GIS Mapping of Earthquake-Related Deaths and Hospital Admissions from the 1994 Northridge, California, Earthquake". In: *Annals of Epidemiology* 10.1 (Jan. 2000), pp. 5–13. ISSN: 10472797. DOI: 10.1016/S1047-2797(99)00058-7. URL: https://linkinghub.elsevier.com/retrieve/pii/S1047279799000587 (visited on 10/15/2023).

[4] Luis Ceferino et al. "Effective plans for hospital system response to earthquake emergencies". In: *Nature Communications* 11.1 (Dec. 2020). Publisher: Springer US, p. 4325. ISSN: 2041-1723. DOI: 10.1038/s41467-020-18072-w. URL: http://dx.doi.org/10.1038/s41467-020-18072-w.

[5] Luis Ceferino et al. "Placing engineering in the earthquake response and the survival chain". en. In: *Nature Communications* 15.1 (May 2024), p. 4298. ISSN: 2041-1723. DOI: 10.1038/s41467-024-48624-3. URL: https://www.nature.com/articles/s41467-024-48624-3 (visited on 01/07/2025).

[6] Yvonne Merino et al. "Modeling hospital resources based on global epidemiology after earthquake-related disasters". en. In: *Earthquake Spectra* (Aug. 2024), p. 87552930241262788. ISSN: 8755-2930, 1944-8201. DOI: 10.1177/87552930241262788. URL: https://journals.sagepub.com/doi/10.1177/87552930241262788 (visited on 09/30/2024).

[7] A W Coburn, R J S Spence, and A Pomonis. "Factors determining human casualty levels in earthquakes: Mortality prediction in building collapse". In: *Earthquake Engineering, Tenth World Conference*. Vol. 10. Balkema Rotterdam, 1992, pp. 5989–5994.

[8] Derek C. Angus et al. "Epidemiologic Assessment of Mortality, Building Collapse Pattern, and Medical Response after the 1992 Earthquake in Turkey". en. In: *Prehospital and Disaster Medicine* 12.3 (Sept. 1997), pp. 49–58. ISSN: 1049-023X, 1945-1938. DOI: 10.1017/S1049023X0003764X. URL: https://www.cambridge.org/core/product/identifier/S1049023X0003764X/type/journal_article (visited on 09/25/2025).

[9] E. K. M. So. "Challenges in Collating Earthquake Casualty Field Data". In: *Human Casualties in Earthquakes*. Dordrecht: Springer Netherlands, 2011, pp. 231–254. ISBN: 978-90-481-9454-4. DOI: 10.1007/978-90-481-9455-1_16. URL: http://www.springerlink.com/index/10.1007/978-90-481-9455-1.

[10] R. J. S. Spence and Emily So. *Why do buildings collapse in earthquakes? building for safety in seismic areas*. Hoboken, NJ: Wiley-Blackwell, 2021. ISBN: 978-1-119-61946-8 978-1-119-61945-1.

[11] O.S. Better. "History of the Crush Syndrome: From the Earthquakes of Messina, Sicily 1909 to Spitak, Armenia 1988". en. In: *American Journal of Nephrology* 17.3-4 (1997), pp. 392–394. ISSN: 1421-9670, 0250-8095. DOI: 10.1159/000169127. URL: https://www.karger.com/Article/FullText/169127 (visited on 09/03/2023).

[12] C Peek-Asa et al. "Seismic, structural, and individual factors associated with earthquake related injury". en. In: *Injury Prevention* 9.1 (Mar. 2003), pp. 62–66. ISSN: 1353-8047, 1475-5785. DOI: 10.1136/ip.9.1.62. URL: https://injuryprevention.bmj.com/lookup/doi/10.1136/ip.9.1.62 (visited on 09/25/2025).

[13] M. Bulut et al. "Medical experience of a university hospital in Turkey after the 1999 Marmara earthquake". In: *Emergency Medicine Journal* 22.7 (July 2005), pp. 494–498. ISSN: 1472-0205. DOI: 10.1136/emj.2004.016295. URL: https://emj.bmj.com/lookup/doi/10.1136/emj.2004.016295.

[14] Wenfang Li et al. "Management of severe crush injury in a front-line tent ICU after the 2008 Wenchuan earthquake in China: an experience with 32 cases." In: *Critical Care* 13.6 (2009). ISBN: 1466-609X (Electronic)\r1364-8535 (Linking), R178. ISSN: 1466-609X. DOI: 10.1186/cc8160. URL: http://www.ncbi.nlm.nih.gov/pubmed/19895693.

[15] Ting Li et al. "Orthopaedic injury analysis in the 2010 Yushu, China Earthquake". In: *Injury* 43.6 (2012). Publisher: Elsevier Ltd ISBN: 1879-0267, pp. 886–890. ISSN: 00201383. DOI: 10.1016/j.injury.2011.11.020. URL: http://dx.doi.org/10.1016/j.injury.2011.11.020.

[16] Milt Statheropoulos et al. "Factors that affect rescue time in urban search and rescue (USAR) operations". In: January (2015). DOI: 10.1007/s11069-014-1304-3.

[17] Hıdır Sarı et al. “First-Week Analysis after the Turkey Earthquakes: Demographic and Clinical Outcomes of Victims”. en. In: *Prehospital and Disaster Medicine* 38.3 (June 2023), pp. 294–300. ISSN: 1049-023X, 1945-1938. DOI: 10.1017/S1049023X23000493. URL: https://www.cambridge.org/core/product/identifier/S1049023X23000493/type/journal_article (visited on 10/03/2023).

[18] Shih-Tien Pan et al. “Association of injury pattern and entrapment location inside damaged buildings in the 2016 Taiwan earthquake”. en. In: *Journal of the Formosan Medical Association* 118.1 (Jan. 2019), pp. 311–323. ISSN: 09296646. DOI: 10.1016/j.jfma.2018.05.012. URL: https://linkinghub.elsevier.com/retrieve/pii/S0929664618300822 (visited on 09/03/2023).

[19] Gregory G Deierlein et al. “ATC 63 Methodology for Evaluating Seismic Collapse Safety of Archetype Buildings”. In: (2008).

[20] Abbie Liel. “Assessing the collapse risk of California’s existing reinforced concrete frame structures: Metrics for seismic safety decisions”. PhD thesis. Stanford University, 2008.

[21] Gregory Deierlein and Abbie Liel. “Benefit–Cost Evaluation of Seismic Risk Mitigation in Existing Non-ductile Concrete Buildings”. In: *Advances in Performance-Based Earthquake Engineering. Geotechnical, Geological and Earthquake Engineering*. Ed. by Fardis M. Vol. 13. ISSN: 15736059. Dordrecht: Springer, 2010. ISBN: 978-90-481-8745-4. DOI: 10.1007/978-90-481-8746-1.

[22] Curt B. Haselton et al. “Seismic Collapse Safety of Reinforced Concrete Buildings. I: Assessment of Ductile Moment Frames”. In: *Journal of Structural Engineering* 137.4 (2011), pp. 481–491. ISSN: 0733-9445. DOI: 10.1061/(asce)st.1943-541x.0000318.

[23] Abbie B. Liel, Curt B. Haselton, and Gregory G. Deierlein. “Seismic Collapse Safety of Reinforced Concrete Buildings. II: Comparative Assessment of Nonductile and Ductile Moment Frames”. en. In: *Journal of Structural Engineering* 137.4 (Apr. 2011), pp. 492–502. ISSN: 0733-9445, 1943-541X. DOI: 10.1061/(ASCE)ST.1943-541X.0000275. URL: https://ascelibrary.org/doi/10.1061/%28ASCE%29ST.1943-541X.0000275 (visited on 09/03/2023).

[24] Siamak Sattar and Abbie B. Liel. “Seismic performance of nonductile reinforced concrete frames with masonry infill walls - I: Development of a strut model enhanced by finite element models”. In: *Earthquake Spectra* 32.2 (2016), pp. 795–818. ISSN: 87552930. DOI: 10.1193/90914EQS139M.

[25] Kenneth Elwood and Jack Moehle. “Axial Capacity Model for Shear-Damaged Columns”. en. In: *ACI Structural Journal* 102.4 (2005). ISSN: 0889-3241. DOI: 10.14359/14562. URL: http://www.concrete.org/Publications/ACIMaterialsJournal/ACIJournalSearch.aspx?m=details&ID=14562 (visited on 09/25/2025).

[26] Kenneth J. Elwood and Jack P. Moehle. “Drift Capacity of Reinforced Concrete Columns with Light Transverse Reinforcement”. en. In: *Earthquake Spectra* 21.1 (Feb. 2005), pp. 71–89. ISSN: 8755-2930, 1944-8201. DOI: 10.1193/1.1849774. URL: https://journals.sagepub.com/doi/10.1193/1.1849774 (visited on 09/25/2025).

[27] E. Tapia-Hernández, M.C. Genes, and H. Guerrero-Bobadilla. "Damages Observed in Turkey Due to the Kahramanmaras Earthquakes of February 6, 2023". en. In: *Journal of Earthquake Engineering* (May 2024), pp. 1–19. ISSN: 1363-2469, 1559-808X. DOI: 10.1080/13632469.2024.2353870. URL: https://www.tandfonline.com/doi/full/10.1080/13632469.2024.2353870 (visited on 09/25/2025).

[28] Abdullah Dilsiz et al. *StEER: 2023 Mw 7.8 Kahramanmaras, Türkiye Earthquake Sequence Preliminary Virtual Reconnaissance Report (PVRR)*. en. Tech. rep. DesignsafeCI, 2023. URL: https://www.designsafe-ci.org/data/browser/public/designsafe.storage.published/PRJ-3824v2/#details-9427328110404521l5-242ac11b-0001-012 (visited on 08/24/2023).

[29] Y. Aktaş et al. *The Türkiye Earthquake Sequence of February 2023: A Longitudinal Study Report by EEFIT. Earthquake Engineering Field Investigation Team (EEFIT)*. Tech. rep. Institution of Structural Engineers (IStructE), 2024. URL: 10.13140/RG.2.2.15906.40641.

[30] Hope Seligson, Kimberley I. Shoaf, and Mahue-Giangreco. "Engineering-Based Earthquake Casualty Modeling: Past, Present and Future". In: *7th National Conference on Earthquakes, Earthquake Engineering Research Institute*. Boston, MA, 2002.

[31] Keith Porter, Kim Shoaf, and Hope Seligson. "Value of injuries in the Northridge earthquake". In: *Earthquake Spectra* 22.2 (2006), pp. 555–563. ISSN: 87552930. DOI: 10.1193/1.2194529.

[32] David J. Wald et al. "Advancements in Casualty Modelling facilitated by the USGS Prompt Assessment of global earthquakes for response (PAGER) system". In: *Second International Workshop on Disaster Casualties*. Issue: June. University of Cambridge, UK, 2009, pp. 221–230. ISBN: 978-90-481-9454-4. DOI: 10.1007/978-90-481-9455-1_15. URL: http://www.springerlink.com/index/10.1007/978-90-481-9455-1.

[33] T. I. Allen et al. "PAGER-CAT: A Composite Earthquake Catalog for Calibrating Global Fatality Models". In: *Seismological Research Letters* 80.1 (2009), pp. 57–62. ISSN: 0895-0695. DOI: 10.1785/gssrl.80.1.57.

[34] Kristin D. Marano, David J. Wald, and Trevor I. Allen. "Global earthquake casualties due to secondary effects: A quantitative analysis for improving rapid loss analyses". In: *Natural Hazards* 52.2 (2010). ISBN: 0921-030X\r1573-0840, pp. 319–328. ISSN: 0921030X. DOI: 10.1007/s11069-009-9372-5.

[35] K. S. Jaiswal et al. "Earthquake Casualty Models Within the USGS Prompt Assessment of Global Earthquakes for Response (PAGER) System". In: *Human Casualties in Earthquakes*. 2011. ISBN: 978-90-481-9454-4.

[36] K. Shoaf and H. Seligson. "Estimating Casualties for the Southern California ShakeOut". In: *Human Casualties in Earthquakes: Progress in Modelling and Mitigation*. Springer, 2011, pp. 125–137. ISBN: 978-90-481-9455-1. DOI: 10.1007/978-90-481-9455-1.

[37] H Y Noh et al. "Bayesian Updating of Earthquake Vulnerability Functions with Application to Mortality Rates". In: *Earthquake Spectra* 33.3 (2017), pp. 1173–1189. ISSN: 8755-2930. DOI: 10.1193/081216EQS133M.

[38] Luis Ceferino, Anne Kiremidjian, and Gregory Deierlein. "Probabilistic Model for Regional Multiseverity Casualty Estimation due to Building Damage Following an Earthquake". In: *ASCE-ASME Journal of Risk and Uncertainty in Engineering Systems, Part A: Civil Engineering* 4.3 (Sept. 2018), p. 04018023. ISSN: 2376-7642. DOI: 10.1061/AJRUA6.0000972. URL: http://ascelibrary.org/doi/10.1061/AJRUA6.0000972.

[39] Luis Ceferino, Anne Kiremidjian, and Gregory Deierlein. "Regional Multiseverity Casualty Estimation Due to Building Damage following a Mw 8.8 Earthquake Scenario in Lima, Peru". In: *Earthquake Spectra* 34.4 (Nov. 2018), pp. 1739–1761. ISSN: 8755-2930. DOI: 10.1193/080617EQS154M. URL: http://journals.sagepub.com/doi/10.1193/080617EQS154M.

[40] Applied Technology Council (ATC). *ATC-13. Earthquake damage evaluation data for California*. Tech. rep. ISBN: 0915-5805. Redwood City, CA: Applied Technology Council (ATC), 1985, p. 492. URL: http://nisee.berkeley.edu/elibrary/Text/S22323.

[41] Federal Emergency Management Agency (FEMA). *Hazus Earthquake Model, Technical Manual (Hazus 4.2 SP3)*. Tech. rep. Issue: October. Washington, DC: Federal Emergency Management Agency, 2020.

[42] Marla Ann Petal. *Urban disaster mitigation and preparedness: the 1999 Kocaeli earthquake*. eng. OCLC: 103988806. 2004. ISBN: 978-0-496-00323-5.

[43] Marla Petal et al. *Research Report: Causes of Deaths and Injuries in the 2015 Gorkha (Nepal) Earthquake*. Tech. rep. Kathmandu: Save the Children, 2017.

[44] Federal Emergency Management Agency (FEMA). *Seismic Performance Assessment of Buildings, Volume 1 – Methodology, Technical report FEMA-P58*. Tech. rep. Washington, DC, 2012.

[45] Federal Emergency Management Administration. *Seismic Performance Assessment of Buildings, Volume 2 – Implementation Guide, Technical report FEMA-P58*. en. Tech. rep. Washington DC, 2018.

[46] Antonios Pomonis, Emily So, and Jim Cousins. "Assessment of fatalities from the Christchurch, New Zealand Earthquake of February 22nd, 2011". en. In: (2011). Publisher: Unpublished. DOI: 10.13140/RG.2.1.2191.3687. URL: http://rgdoi.net/10.13140/RG.2.1.2191.3687 (visited on 09/03/2023).

[47] Emily So. *Estimating Fatality Rates for Earthquake Loss Models*. 1st ed. 2016. SpringerBriefs in Earth Sciences. Cham: Springer International Publishing : Imprint: Springer, 2016. ISBN: 978-3-319-26838-5. DOI: 10.1007/978-3-319-26838-5.

[48] Carlo P. Campobasso, Rosa Falamingo, and Francesco Vinci. "Investigation of Italy's deadliest building collapse: forensic aspects of a mass disaster". eng. In: *Journal of Forensic Sciences* 48.3 (May 2003), pp. 635–639. ISSN: 0022-1198.

[49] Christine Schweier and Michael Markus. "Classification of Collapsed Buildings for Fast Damage and Loss Assessment". en. In: *Bulletin of Earthquake Engineering* 4.2 (May 2006), pp. 177–192. ISSN: 1570-761X, 1573-1456. DOI: 10.1007/s10518-006-9005-2. URL: http://link.springer.com/10.1007/s10518-006-9005-2 (visited on 09/25/2025).

[50] Emily So, Hannah Baker, and Robin Spence. "CASUALTY ESTIMATION THROUGH ASSESSMENT OF VOLUME LOSS AND EXTERNAL DEBRIS SPREAD IN BUILDING COLLAPSE". In: *16th European Conference on Earthquake Engineering*. Thessaloniki, 2018.

[51] G Deierlein, Andrei Reinhorn, and Michael Wilford. *Nonlinear Structural Analysis For Seismic Design: A Guide for Practicing Engineers*. Tech. rep. NIST GCR 10-917-5. 2010. URL: https://nehrp.gov/pdf/nistgcr10-917-5.pdf.

[52] David Lallemant, Anne Kiremidjian, and Henry Burton. "Statistical procedures for developing earthquake damage fragility curves". en. In: *Earthquake Engineering & Structural Dynamics* 44.9 (July 2015). Publisher: Wiley, pp. 1373–1389. ISSN: 0098-8847, 1096-9845. DOI: 10.1002/eqe.2522. URL: https://onlinelibrary.wiley.com/doi/10.1002/eqe.2522 (visited on 07/11/2025).

[53] Mabé Villar-Vega et al. "Development of a Fragility Model for the Residential Building Stock in South America". In: *Earthquake Spectra* 33.2 (2017), 010716EQS005M. ISSN: 8755-2930. DOI: 10.1193/010716EQS005M. URL: http://earthquakespectra.org/doi/10.1193/010716EQS005M.

[54] Luis Moya et al. "Novel unsupervised classification of collapsed buildings using satellite imagery, hazard scenarios and fragility functions". In: *Remote Sensing* 10.2 (2018). ISSN: 20724292. DOI: 10.3390/rs10020296.

[55] Maja Kucharczyk and Chris H. Hugenholtz. "Pre-disaster mapping with drones: an urban case study in Victoria, British Columbia, Canada". en. In: *Natural Hazards and Earth System Sciences* 19.9 (Sept. 2019), pp. 2039–2051. ISSN: 1684-9981. DOI: 10.5194/nhess-19-2039-2019. URL: https://nhess.copernicus.org/articles/19/2039/2019/ (visited on 09/29/2025).

[56] Ilaria Tonti et al. "Digitalization and Spatial Documentation of Post-Earthquake Temporary Housing in Central Italy: An Integrated Geomatic Approach Involving UAV and a GIS-Based System". en. In: *Drones* 7.7 (July 2023), p. 438. ISSN: 2504-446X. DOI: 10.3390/drones7070438. URL: https://www.mdpi.com/2504-446X/7/7/438 (visited on 09/29/2025).

[57] Dongfeng Jia, Yanping Liu, and Lishuo Zhang. "A rapid evaluation method of the seismic damage to buildings based on UAV images". en. In: *Geomatica* 76.1 (July 2024), p. 100006. ISSN: 11951036. DOI: 10.1016/j.geomat.2024.100006. URL: https://linkinghub.elsevier.com/retrieve/pii/S1195103624000065 (visited on 09/29/2025).

[58] Fumio Yamazaki, Wen Liu, and Yoshihisa Maruyama. "Landslide Extraction from Airborne Lidar Data in the 2018 Hokkaido-Eastern-Iburi Earthquake". In: *IGARSS 2024 - 2024 IEEE International Geoscience and Remote Sensing Symposium*. Athens, Greece: IEEE, July 2024, pp. 380–383. ISBN: 979-8-3503-6032-5. DOI: 10.1109/IGARSS53475.2024.10640403. URL: https://ieeexplore.ieee.org/document/10640403/ (visited on 09/29/2025).

[59] Helen Crowley et al. "Framework for Developing Fragility and Consequence Models for Local Personal Risk". en. In: *Earthquake Spectra* 33.4 (Nov. 2017), pp. 1325–1345. ISSN: 8755-2930, 1944-8201. DOI: 10.1193/083116eqs140m. URL: https://journals.sagepub.com/doi/10.1193/083116eqs140m (visited on 09/25/2025).

[60] Michael E. Durkin. *Fatalities, nonfatal injuries and medical aspects of the Northridge earthquake, Northridge, California earthquake of 17 January 1994*. Tech. rep. California Department of Conservation, Division of Mines and Geology, 1995, pp. 247–254.

[61] Corinne Peek-Asa et al. "Fatal and hospitalized injuries resulting from the 1994 Northridge earthquake". In: *International Journal of Epidemiology* 27.3 (1998), pp. 459–465. ISSN: 03005771. DOI: 10.1093/ije/27.3.459.

[62] Michael E. Durkin et al. "Injuries and emergency medical response in the Loma Prieta earthquake". In: *Bulletin of the Seismological Society of America* 81.5 (1991), pp. 2143–2166. ISSN: 1943-3573. URL: http://bssa.geoscienceworld.org/content/81/5/2143.abstract.

[63] Michele Nguyen and David Lallemant. "Order Matters: The Benefits of Ordinal Fragility Curves for Damage and Loss Estimation". In: *Risk Analysis* 0.0 (2021). ISSN: 15396924. DOI: 10.1111/risa.13815.

[64] James A. Mahaney et al. "The capacity spectrum method for evaluating structural response during the Loma Prieta earthquake". In: *National Earthquake Conference*. 1993, pp. 501–510. URL: http://bases.bireme.br/cgi-bin/wxislind.exe/iah/online/?IsisScript=iah/iah.xis&src=google&base=DESASTRES&lang=p&nextAction=lnk&exprSearch=6697&indexSearch=ID.

[65] Volkan Karabacak et al. "The 2023 Pazarcık (Kahramanmaraş, Türkiye) earthquake (M_w 7.7): implications for surface rupture dynamics along the East Anatolian Fault Zone". en. In: *Journal of the Geological Society* 180.3 (May 2023), jgs2023–020. ISSN: 0016-7649, 2041-479X. DOI: 10.1144/jgs2023-020. URL: https://www.lyellcollection.org/doi/10.1144/jgs2023-020 (visited on 09/26/2025).

[66] Yijun Zhang et al. "Geometric controls on cascading rupture of the 2023 Kahramanmaraş earthquake doublet". en. In: *Nature Geoscience* 16.11 (Nov. 2023), pp. 1054–1060. ISSN: 1752-0894, 1752-0908. DOI: 10.1038/s41561-023-01283-3. URL: https://www.nature.com/articles/s41561-023-01283-3 (visited on 09/26/2025).

[67] The Independent. *Watch Again: View from Hatay after third quake hits Turkey*. 2023. URL: https://www.youtube.com/watch?v=QkSjKtSj7Ls&ab_channel=TheIndependent (visited on 09/25/2025).

[68] Kuşbakışı. *Hatay Defne 10 Şubat 2023 Deprem Bölgesi 360 Derece*. 2023. URL: https://aydinsanaltur.com/deprem/hataydefne/ (visited on 09/25/2025).

[69] A. [@alpersener] Şener. *Antakya Deprem sonrası Saray Caddesi ve Cumhuriyet Meydanı [Instagram Video]*. tr. 2023. URL: https://www.instagram.com/reel/Cp8GvxJM05g/?igsh=MTIxZXEyaGE5anRjMA== (visited on 09/25/2025).

[70] A. [@alpersener] Şener. *Sağ tarafta gördüğünüz yapı Asia Cafe ve bu yol Eski Antakya Sokaklarına giden o dar yol. Bir zamanlar cıvıl cıvıl olan bu sokaklarda artık yıkıntılar var... [Instagram Video]*. tr. 2023. URL: https://www.instagram.com/reel/Cpnd4njIcdz/?igsh=amE4dWxxM25mZ2J10 (visited on 09/25/2025).

[71] Guardian News. *Aerial footage shows earthquake aftermath in hard-hit Turkish region of Hatay*. 2023. URL: https://www.youtube.com/watch?v=Gn4Dm6CR6XE&ab_channel=GuardianNews (visited on 09/25/2025).

[72] Demirören Haber Ajansı. *Depremin Vurduğu Malatya Havadan Görüntülendi*. 2023. URL: https://youtu.be/55kLYZlShto?si=Ez1kZvhA-hfsaPM3 (visited on 09/25/2025).

[73] NTV. *Malatya'daki yıkımı NTV drone kamerası görüntüledi*. 2023. URL: https://youtu.be/j5ykHdNFfpo?si=7ngFz4EQSo0nN-yT (visited on 09/25/2025).

[74] Breaking News King [@breakingnewsking]. *Malatya city in Turkey after the earthquake #shorts*. 2023. URL: https://www.youtube.com/shorts/cbPbvB8m7mg (visited on 09/25/2025).

[75] Maxar. *Turkey Earthquake: Analysis-Ready Data (ARD)*. 2023. URL: https://www.maxar.com/open-data/turkey-earthquake (visited on 10/02/2023).

[76] David J. Wald et al. "ShakeMap operations, policies, and procedures". In: *Earthquake Spectra* 38.1 (2022). ISBN: 8755293021103, pp. 756–777. ISSN: 19448201. DOI: 10.1177/87552930211030298.

[77] C. Bruce Worden et al. "Spatial and Spectral Interpolation of Ground-Motion Intensity Measure Observations". en. In: *Bulletin of the Seismological Society of America* 108.2 (Apr. 2018), pp. 866–875. ISSN: 0037-1106, 1943-3573. DOI: 10.1785/0120170201. URL: https://pubs.geoscienceworld.org/ssa/bssa/article/108/2/866/528138/Spatial-and-Spectral-Interpolation-of-GroundMotion (visited on 09/26/2025).

[78] American Society of Civil Engineers. *Minimum Design Loads and Associated Criteria for Buildings and Other Structures*. en. Reston, VA: American Society of Civil Engineers, Nov. 2021. ISBN: 978-0-7844-1578-8 978-0-7844-8349-7. DOI: 10.1061/9780784415788. URL: https://ascelibrary.org/doi/book/10.1061/9780784415788 (visited on 09/26/2025).